Advances in Science and Technology Research Journal

Advances in Science and Technology Research Journal, 18(6), 177–188
https://doi.org/10.12913/22998624/191263
ISSN 2299-8624, License CC-BY 4.0

Received: 2024.06.12
Accepted: 2024.07.16
Published: 2024.09.08

Development of the Design of an Experimental Adsorber and Optimization of its Gas-Dynamic Parameters

Vasyl Mykhailiuk[1], Damian Dzienniak[2*], Yevstakhiy Kryzhanivskyy[1], Ruslan Deineha[1], Roman Stetsiuk[1], Andrzej Uhryński[3], Tomasz Rokita[4]

[1] Department of Oil and Gas Field Machinery and Equipment, Ivano-Frankivsk National Technical University of Oil and Gas, Karpatska St. 15, Ivano-Frankivsk, 76019, Ukraine

[2] Department of Manufacturing Systems, Faculty of Mechanical Engineering and Robotics, AGH University of Krakow, A. Mickiewicza 30, 30-059 Krakow, Poland

[3] Department of Machine Design and Maintenance, Faculty of Mechanical Engineering and Robotics, AGH University of Krakow, A. Mickiewicza 30, 30-059 Krakow, Poland

[4] Departament of Mechinery Engineering and Transport, Faculty of Mechanical Engineering and Robotics, AGH University of Krakow, A. Mickiewicza 30, 30-059 Krakow, Poland

* Corresponding author's e-mail: ddamian@agh.edu.pl

ABSTRACT

Various technologies and equipment are used to reduce greenhouse gas emissions. For example, the method of adsorption is used to capture carbon dioxide (CO_2) from the smoke emissions of cement industries. In the adsorption process using zeolites, devices such as adsorbers are typically employed. Zeolites, a versatile group of aluminosilicate materials, are known for their high surface area and selective adsorption properties, making them effective for CO_2 capture. The effectiveness of the adsorber depends on many factors, including its geometric dimensions and shape. Adsorbers with a central inlet flow have uneven gas distribution at the entrance to the adsorbent layer, which reduces their operational efficiency. To eliminate this disadvantage, various devices installed at the output of the adsorber inlet are usually used. Analysis of such devices shows that they do not provide maximum adsorption efficiency. To study the efficiency of zeolite operation for capturing carbon dioxide contained in the smoke gases of cement industries, the design of a laboratory adsorber was proposed, featuring a cyclone and distribution device in its lower part. The cyclone prevents the adsorbent from being contaminated by drip fluid, which reduces the efficiency of the adsorption process in the gas, and the distribution device reduces the uniformity of gas distribution at the entrance to the adsorbent layer. This paper proposes a computational fluid dynamics (CFD) model and design of the distribution device, which was analyzed and modified to significantly increase the uniform distribution of gas at the entrance to the adsorbent layer. Compared with other designs of distribution devices, the proposed design is simpler and performs better under varying gas flow rates.

Keywords: carbon dioxide, adsorbent, zeolite, adsorber, speed, efficiency, computational fluid dynamics.

INTRODUCTION

Global warming, caused by increasing environmental pollution, necessitates a radical shift toward a more sustainable energy system and environmentally friendly methods of industrial production, in particular those reducing CO_2 emissions [1–3]. The capture and storage of CO_2 using the adsorption method are widely employed by various industries, including cement production [4]. The choice of adsorbent for capturing CO_2 depends on many factors, such as its efficiency, cost, and availability [3, 5, 6].

Among the variety of materials that are used as adsorbents, one that is inexpensive and commonly used is zeolite [7, 8]. In the adsorption

process using zeolite, devices referred to as adsorbers are typically employed. They are divided into different categories: fixed granular adsorbers, moving granular adsorbers, and those with a fluidized (pseudo-liquid) layer of fine dispersed adsorbent [9]. The effectiveness of the adsorber depends on various factors, including its geometric dimensions and shape [10–12].

Vertical adsorbers face challenges in ensuring the uniform distribution of gas flow rates across the cross-section of the inlet to the bulk working layer [13–15]. The gas enters through a nozzle with a cross-sectional area 15–50 times smaller than that of the housing, leading to uneven distribution of speed and pressure [9]. This results in uneven gas flow through the adsorbent layer. In one part of the layer, the movement of gas is accelerated, and in the other, it slows down, which leads to a decrease in the overall efficiency of the adsorber.

Understanding the adsorption properties of different materials is crucial for optimizing the capture and storage of gases. For instance, the nitrogen adsorption–desorption behavior of carbon materials derived from coffee waste, as investigated in other studies, provides insight into the physical sorption characteristics and surface area metrics that are critical for effective adsorption processes [16]. Similarly, porous carbon materials (PCMs) have been studied for their multifunctional applications, including energy storage, owing to their unique structural and electrochemical properties [17]. These studies show that the adsorption isotherms and the specific surface area of the materials play a significant role in their efficiency as adsorbents. By examining such properties, one can draw parallels and improve the selection and design of adsorbents for CO_2 capture.

In order to achieve even distribution of the gas flow across the adsorber cross-section before the working layer, distribution devices are placed at the outlet of the gas flow from the inlet nozzle [15]. The most common ones consist of a flat disk screen installed below the input nozzle. The gas stream from the inlet pipe hits the flat screen, changing its direction of movement. The disk screen is attached to the inlet pipe with a special frame or ribs welded to the expansion nozzle or directly to the bottom of the adsorber. The efficiency of gas flow distribution using a distribution device directly depends on its geometric dimensions and the ratio of the cross-sectional area of the adsorber housing to that of the inlet nozzle [18, 19]. A higher area ratio demands greater efficiency in gas flow distribution created by the device [20]. The efficiency of gas flow distribution also depends on the size of the distribution device and the relative distance between the device (at the stream inlet) and the working layer of the adsorbent. This design does not ensure a uniform distribution of the gas flow across the cross-section of the adsorber at the entrance to the bulk layer of the adsorbent, reducing the adsorption capacity by 30%.

There are also diffuser types of distribution devices [21]. These improve the uniformity of gas flow distribution in the adsorber cross-section in comparison with the disk screen by allowing preliminary expansion of the flow in the diffuser. Smooth output and subsequent expansion in the space beneath the adsorbent layer are crucial. However, diffusers alone cannot achieve sufficiently uniform gas flow distribution, leading to variable speeds at different cross-sectional points and the occurrence of reverse flow in the areas with reduced static pressure [22].

Additionally, a distribution device is used to enhance gas flow distribution at the entrance to the adsorbent layer [23]. This device, placed in the input nozzle, contains two concentric rings of different diameters and a flat disk screen. While this design slightly increases the efficiency of gas flow distribution, it also presents certain disadvantages: 1) the distribution device is too tall; 2) the design becomes more complex [24].

The purpose of the work was to use fluid simulation to design an experimental adsorber with a specific shape and size of internal elements to improve its efficiency. The primary objectives were: 1) to develop the design of the experimental CO_2 adsorber based on a comprehensive analysis, with consideration of the unique aspects of cement production; 2) to select and optimize the design of its internal elements for improved performance.

Cement production is an energy-intensive and expensive process that yields one of the most popular and essential building materials [25–27]. Cement can be used both independently and as a component in other materials [28, 29]. During its production, raw materials like limestone and clay are mixed in a specific ratio (75–80% limestone and 20–25% clay). This mixture closely resembles natural marl (a limestone-clay rock) in composition. Cement can be produced in three ways: wet, dry, and combined.

In the wet process, all types of raw materials, after grinding, are mixed and then ground in an aquatic environment in special mills. The resulting sludge (a dense suspension containing 35–40% water) enters large pools, where it is thoroughly mixed. The cement mixture is then burned in a rotating furnace, shaped like a drum with a diameter of up to 5 meters and lined with refractory material. The sludge is continuously fed into the furnace. The movement of flue gases, a by-product of combustion, occurs within the system. This motion is facilitated by the inclined orientation and slow rotation of the furnace, directing the resultant mixture toward the combustion point.

As the mixture of calcium carbonate undergoes thermal decomposition, yielding calcium oxide and carbon dioxide, the process of clay decomposition is also initiated. At temperatures of approximately 1500 °C, calcium oxide reacts with the constituents of clay, forming silicates, aluminosilicates, calcium aluminates, and other assorted products. After the firing process, the resultant clinker is pulverized alongside gypsum in specialized cylindrical ball mills, where steel balls facilitate particle size reduction [30–32]. This procedure culminates in the production of cement powder, completing the manufacturing process [33].

Cement production emits various pollutants that negatively impact the environment [34–36]. In order to reduce these emissions, many different technologies and entire equipment complexes have been developed. However, such technologies and complexes are expensive both in the manufacture as well as during operation and maintenance.

When it comes to utilization and application of captured CO_2 and other harmful impurities extracted from flue gases, the condensate from flue gases with partially dissolved CO_2 and small mechanical harmful particles can be utilized in cement slurry and used both for the production of concrete products as well as in the process of constructing oil and gas wells. Using flue gas condensate for making cement stone results in improved mechanical properties [37, 38]. Another option for CO_2 application is its transportation through pipelines for injection into depleted oil and gas reservoirs [39, 40]. Their advantages include an effective structure that retains hydrocarbons and can also retain carbon dioxide. Among the known methods of using CO_2 is its use to enhance hydrocarbon recovery from oil and gas fields at various stages of extraction [41, 42]. This process includes maintaining reservoir pressure, extracting residual oil from watered-out oil reservoirs, and recovering condensed hydrocarbons from depleted gas-condensate reservoirs [43]. An effective technology is injecting CO_2 into formations with high-viscosity oil to increase oil recovery [44]. CO_2 has a unique and extremely beneficial property for increasing oil production, namely the ability to increase the viscosity of water when dissolved in it [45]. These properties of carbon dioxide are extremely important when developing fields with high-viscosity oil. Injecting CO_2 into oil reservoirs is considered one of the most effective methods for oil extraction and reducing CO_2 emissions [46].

Ensuring the uniform distribution of the incoming gas flow across the adsorber cross-section before the bulk layer of the adsorbent, especially with the central arrangement of the connecting pipe, is a critical objective not only for adsorbers, but also for other devices, such as filters, separators, and furnaces [15]. An analysis of the efficiency of existing distribution devices shows that the known design structures are largely ineffective.

MATERIALS AND METHODS

Adsorber construction

The article proposes to remove the water vapor from the smoke gases of cement production (to obtain smoke condensate). To achieve this, a "method of release of fluid and mechanical impurities from the gas flow" is developed in the work [47]. The main task of this method is to increase the efficiency of the purification of flue gases in large volumes of water vapor and mechanical impurities to ensure environmental safety. When using this method of allocation of water and mechanical particles from high-temperature gas flow (120–160 °C) is carried out with minimal energy consumption. The resulting smoke condensate will be disposed of or reused in the process of cement production.

To implement the proposed method, taking into account the composition and various characteristics of the flue gases from cement production, a multi-nozzle device and a gas-liquid separator have been developed [47]. As the flue gases pass through the multi-nozzle device, their cooling and condensation of water vapor occur, with the condensate being collected using the gas-liquid separator.

To capture carbon dioxide from the cooled flue gases of cement production, it is proposed to pass them through the adsorber structure developed in the laboratory (Figure 1). The main advantages of the developed structure include simplicity, the presence of interchangeable elements, and the ability to capture liquid droplets before the gas flow enters the adsorbent. The presence of liquid droplets in the cooled and purified flue gases from cement production may be due to the specific composition of the flue gases, condensation temperatures, and other factors.

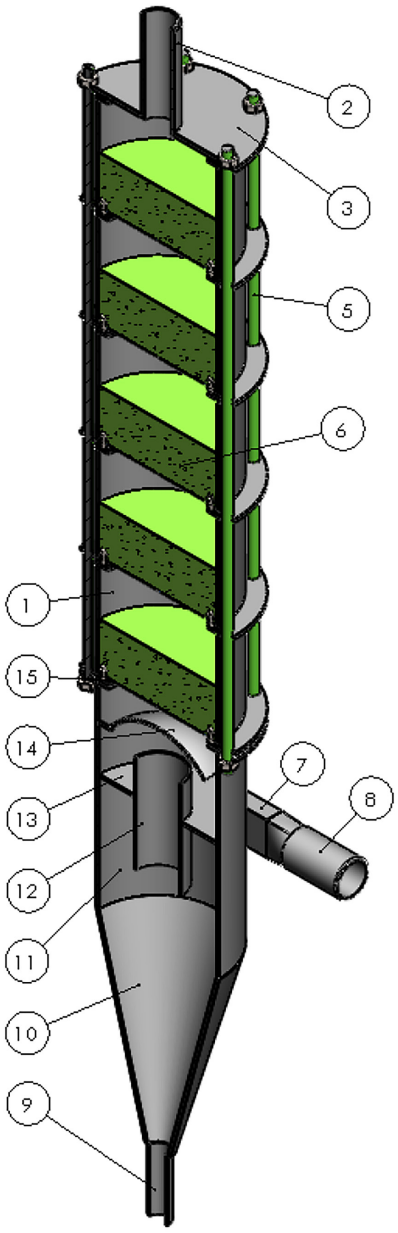

Figure 1. Adsorber construction. Note: 1—housing; 2—outlet nozzle; 3—lid; 4—stud connection; 5—mesh; 6—zeolite; 7—rectangular inlet nozzle; 8—circular inlet nozzle; 9—liquid drain nozzle; 10—conical part of the cyclone housing; 11—cylindrical part of the cyclone housing; 12—cyclone outlet nozzle; 13—disk; 14—deflector; 15—mesh

The structure of the adsorber is as follows. The cylindrical part of the cyclone housing (11) is connected to the conical part of the housing (10), to which the liquid drain nozzle (9) is attached. Inside the cylindrical part of the cyclone housing (11), a disk (13) is placed, which houses the cyclone outlet nozzle (12). A rectangular inlet nozzle (7) is connected to the outside of the cylindrical cyclone housing (11), smoothly transitioning into a circular inlet nozzle (8). At the top, the cylindrical part of the cyclone housing (11) is connected to the adsorber housing (1), in which a mesh (5) is installed to hold the zeolite (6). This construction includes five such adsorber bodies. The number of adsorber bodies can be increased or decreased as necessary. The last (top) adsorber body has a lid (3) with an outlet nozzle (2). The housing (1), lid (3), and the cylindrical part of the cyclone housing (11) are connected by a stud connection (4).

The principle of operation of the laboratory adsorber construction is as follows: the gas-liquid mixture is supplied into the circular inlet nozzle (8) and enters the rectangular inlet nozzle (7). Nozzle (7) is tangentially connected to the cylindrical part of the cyclone housing (11), whereby under the action of centrifugal force and gravitational force, liquid droplets, if present in the gas stream, are separated from it and move downwards, being discharged from the adsorber through the liquid drain nozzle (9).

The gas stream, now free from liquid droplets, moves upwards through the cyclone outlet nozzle (12) and strikes the deflector (14), which alters its direction. After bypassing the deflector (14), the gas stream enters the first adsorption stage, where the adsorbent (zeolite) is located. As the gas passes through the adsorbent, CO_2 is adsorbed, while other components of the gas stream remain unabsorbed.

A distinctive feature of the adsorber construction is the presence of a cyclone in its lower part, which facilitates the removal of liquid from the gas mixture. It is known that the adsorbent used for CO_2 adsorption also absorbs water, significantly reducing the efficiency of CO_2 adsorption [48]. Since the gas flow distribution at the inlet to the adsorbent layer significantly affects the efficiency of the adsorber operation, the article investigated various options for auxiliary devices that promote its uniform distribution.

Flow simulation

The development of various equipment used to rely heavily on the practical experience of researchers, often supplemented by simplified mathematical models. This approach required significant physical and economic resources and frequently failed to yield the desired results. In modern times, with the advancement of computer technology, addressing complex and pressing challenges is inconceivable without the utilization of software suites capable of simulating operational processes occurring within different apparatuses. The study of these processes was extraordinarily labor-intensive and sometimes deemed impossible in practical terms [49–51]. During the development of equipment, software programs implementing CFD methods have gained widespread adoption [52, 53]. One such program is the Flow Simulation module within the SolidWorks software suite [54, 55].

Flow Simulation solves the Navier–Stokes equations, which represent mass, momentum, and energy conservation laws for fluid flows. These equations are enhanced by state equations and empirical dependencies of fluid properties (density, viscosity, and thermal conductivity) on temperature. The viscosity of inelastic non-Newtonian fluids depends on shear rate and temperature, while the density of compressible liquids depends on pressure. Specific problems are defined by geometry, boundary, and initial conditions.

Flow Simulation predicts both laminar and turbulent flows. Laminar flows occur at low Reynolds numbers, defined by velocity, length scale, and kinematic viscosity. Above a critical Reynolds number, flows become turbulent with random fluctuations. Most engineering flows are turbulent, so Flow Simulation focuses on these, using Favre-averaged Navier–Stokes equations to include turbulence effects and employing the k-ε model for turbulence closure.

The same system of equations describes both laminar and turbulent flows, allowing transitions between them. For the models with moving walls, appropriate boundary conditions are specified. For the models with rotating parts, the simulation uses rotating coordinate systems, requiring axisymmetric stationary parts. The conservation laws for mass, momentum, and energy can be written in conservation form in local Cartesian coordinates:

$$\frac{\partial \rho}{\partial t} + \frac{\partial}{\partial x_i}(\rho u_i) = S_M^p \tag{1}$$

$$\frac{\partial \rho u_i}{\partial t} + \frac{\partial}{\partial x_i}(\rho u_i u_j) + \frac{\partial p}{\partial x_i} = \\ = \frac{\partial}{\partial x_i}(\tau_{ij} + \tau_{ij}^R) + S_i + S_{Ii}^p;\ i = 1,2,3;\ j = 1,2,3 \tag{2}$$

$$\frac{\partial \rho H}{\partial t} + \frac{\partial \rho u_i H}{\partial x_i} = \frac{\partial}{\partial x_i}\left[u_j(\tau_{ij} + \tau_{ij}^R) + q_i\right] + \\ + \frac{\partial p}{\partial t} + S_i u_i + S_H^p + Q_H \\ H = h(P,T,y) + \frac{u^2}{2} + k \tag{3}$$

where: u – velocity of the fluid; p – density of the fluid; S_i – mass-distributed external force per unit mass due to a porous media resistance (S_i^{porous}), a gravity ($S_i^{gravity} = \rho g_i$, where g_i is the gravitational acceleration component along the i-th coordinate direction), and the rotation of the coordinate system ($S_i^{rotation}$), i.e., $S_i = S_i^{porous} + S_i^{gravity} + S_i^{rotation}$; H – total enthalpy in the local reference frame; $h(P,T,y)$ – thermal enthalpy at a given pressure (P), temperature (T) and fluid mixture components y; $y = y_1, ..., y_n$ – concentration vector of the fluid mixture components; k – kinetic energy of turbulence; S_M^p, S_{Ii}^p, S_H^p – additional interfacial exchange terms due to Euler-Lagrange particle interaction; Q_H – heat source or sink per unit volume; τ_{ij} – viscous shear stress tensor; q_i – diffusive heat flux.

The subscripts denote summation over the three coordinate directions.

When conducting calculations with the High Mach number flow option activated, the following energy equation is employed:

$$\frac{\partial \rho E}{\partial t} + \frac{\partial \rho u_i \left(E + \frac{p}{\rho}\right)}{\partial x_i} = \\ = \frac{\partial}{\partial x_i}\left[u_j(\tau_{ij} + \tau_{ij}^R) + q_i\right] - \tau_{ij}^R \frac{\partial u_i}{\partial x_i} + \rho\varepsilon + Q_H \\ E = e(\rho,T,y) + \frac{u^2}{2} \tag{4}$$

where: $e(\rho,T,y)$ – internal energy at a given fluid density (ρ), temperature (T), and fluid mixture components (y).

For Newtonian fluids, the viscous shear stress tensor is defined as:

$$\tau_{ij} = \mu\left(\frac{\partial u_i}{\partial x_j} + \frac{\partial u_j}{\partial t_i} - \frac{2}{3}\delta_{ij}\frac{\partial u_k}{\partial x_k}\right) \tag{5}$$

Following Boussinesq assumption, the Reynolds-stress tensor has the following form:

$$\tau_{ij}^{R} = \mu_t \left(\frac{\partial u_i}{\partial x_j} + \frac{\partial u_j}{\partial t_i} - \frac{2}{3}\delta_{ij}\frac{\partial u_k}{\partial x_k} \right) - \frac{2}{3}\rho k \delta_{ij} \quad (6)$$

where: δ_{ij} – Kronecker delta function (equal to unity when $i = j$ but zero otherwise); μ – dynamic viscosity coefficient; μ_t – turbulent eddy viscosity coefficient; k – turbulent kinetic energy.

It should be noted that μ_t and k are equal to zero for laminar flows. Within the framework of the k – turbulence model, μ_t is determined based on two fundamental turbulence characteristics, specifically, the turbulent kinetic energy k and the turbulent dissipation ε:

$$\mu_t = f_\mu \frac{C_\mu \rho k^2}{\varepsilon} \quad (7)$$

where: f_μ – turbulent viscosity factor defined by Equation 8:

$$f_\mu = \left[1 - exp\left(-0.0165 R_y\right)\right]^2 \cdot \left(1 + \frac{20.5}{R_T}\right) \quad (8)$$

where: $R_T = \frac{\rho k^2}{\mu \varepsilon}, R_y = \frac{\rho \sqrt{k} y}{\mu}$ (y – distance from the wall).

This function allows accounting for laminar–turbulent transition.

Two additional transport Equations 9 and 10 are used to describe the turbulent kinetic energy (k) and dissipation (ε):

$$\frac{\partial \rho k}{\partial t} + \frac{\partial}{\partial x_i}(\rho u_i k) = \frac{\partial}{\partial x_i}\left[\left(\mu + \frac{\mu_t}{\sigma_k}\right)\frac{\partial k}{\partial x_i}\right] + S_k \quad (9)$$

$$\frac{\partial \rho \varepsilon}{\partial t} + \frac{\partial}{\partial x_i}(\rho u_i \varepsilon) = \frac{\partial}{\partial x_i}\left[\left(\mu + \frac{\mu_t}{\sigma_\varepsilon}\right)\frac{\partial \varepsilon}{\partial x_i}\right] + S_\varepsilon \quad (10)$$

where: S_k and S_ε are defined as in Equations 11 and 12:

$$S_k = \tau_{ij}^{R}\frac{\partial u_i}{\partial x_j} - \rho\varepsilon + \mu_y P_B \quad (11)$$

$$S_\varepsilon = C_{\varepsilon_1}\frac{\varepsilon}{k}\left(f_1 \tau_{ij}^{R}\frac{\partial u_i}{\partial x_j} + \mu_t C_B P_B\right) - C_{\varepsilon_2} f_2 \frac{\rho \varepsilon^2}{k} \quad (12)$$

where: P_B – turbulent generation caused by buoyancy forces. It can be written as Equation 13:

$$P_B = \frac{g_i}{\sigma_B}\frac{1}{\rho}\frac{\partial \rho}{\partial x_i} \quad (13)$$

where: g_i – component of gravitational acceleration in direction x_i; $\sigma_B = 0.9$, and constant C_B is defined as: $C_B = 1$ when $P_B > 0$, and 0 otherwise.

$$f_1 = 1 + \left(\frac{0.05}{f_\mu}\right);\ f_\mu = 1 - exp(-R_T^2) \quad (14)$$

The constants $C\mu$, $C_{\varepsilon 1}$, $C_{\varepsilon 2}$, σ_k, σ_ε are defined empirically. The following values are typically used in Flow Simulation:

$$C\mu = 0.09,\ C_{\varepsilon 1 =} 1.44,\ C_{\varepsilon 2} = 1.92,$$
$$\sigma_{k =} 1.92,\ \sigma_\varepsilon = 1.3 \quad (15)$$

When the Lewis number $Le = 1$ the diffusive heat flux (q_i) is defined as:

$$q_i = \left(\frac{\mu}{P_r} + \frac{\mu_t}{\sigma_c}\right)\frac{\partial h}{\partial x_i};\ i = 1, 2, 3 \quad (16)$$

where: $\sigma_c = 0.9$; P_r – Prandtl number; h – thermal enthalpy.

These equations encompass both laminar and turbulent flows, with the flexibility for transitions between these states. The parameters k and μ_t are zero for purely laminar flows [56].

RESULTS AND DISCUSSION

For comparison of velocity and pressure distributions on the surface of the first adsorbent layer, simulation modeling of the developed laboratory adsorber was conducted under various gas flow stabilization options at the outlet of the inlet nozzle.

In the initial stage of the investigation, simulation modeling of gas flow was performed without the use of any stabilization devices. The input parameters were set to a pressure of 103 kPa at the inlet of the cyclone and a gas temperature of 75 °C. The gas flow rate at the device outlet was assumed to be 0.13 m^3/s. These input parameter values were determined based on the technological specifications of the equipment to which the adsorber would be connected for its experimental trials.

Considering that the parameters of the technological process may vary during the operation of the adsorber, a parametric study was conducted during the simulation modeling. The gas flow rate was varied from 0.065 m^3/s to 0.26 m^3/s in increments of 0.065 m^3/s.

Figure 2 illustrates the finite element mesh utilized during the simulation modeling. Notably, this mesh featured localized refinement in the device zone to obtain more accurate results. The obtained results, as well as the velocity distribution across the longitudinal section of the cyclone for different gas flow rates, are presented in Figure 3.

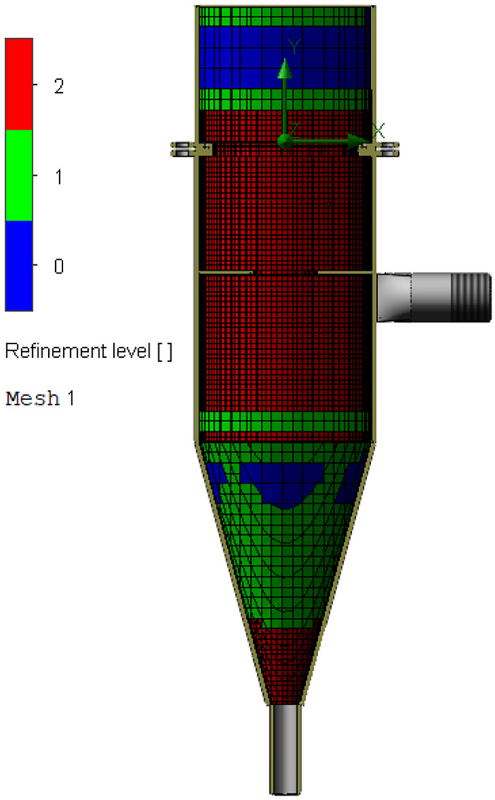

Figure 2. Finite element mesh

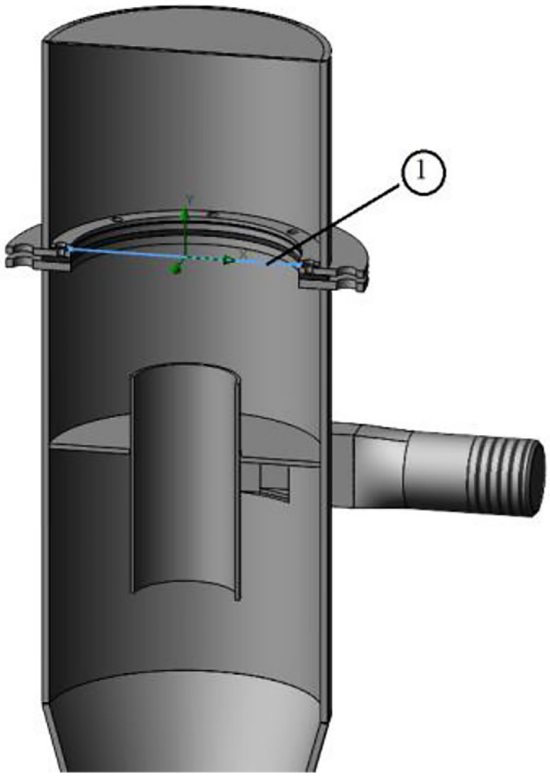

Figure 4. Auxiliary line in cross-section of the cyclone, 1 – auxiliary line

To illustrate the dependency of the change in gas velocity in the cross-section of the cyclone, an auxiliary line was added to the three-dimensional model (Figure 4). Figure 5 displays graphical dependencies illustrating the distribution of gas velocity along the auxiliary line.

On the basis of the results obtained from simulation modeling, it is evident that the velocity distribution across the transverse section of the cyclone is non-uniform. This can be attributed to the operational characteristics of the cyclone, particularly the tangential entry of the gas flow into its housing.

To mitigate this non-uniformity in the velocity distribution across the cross-section of the adsorber, the adoption of a deflector (1) installed

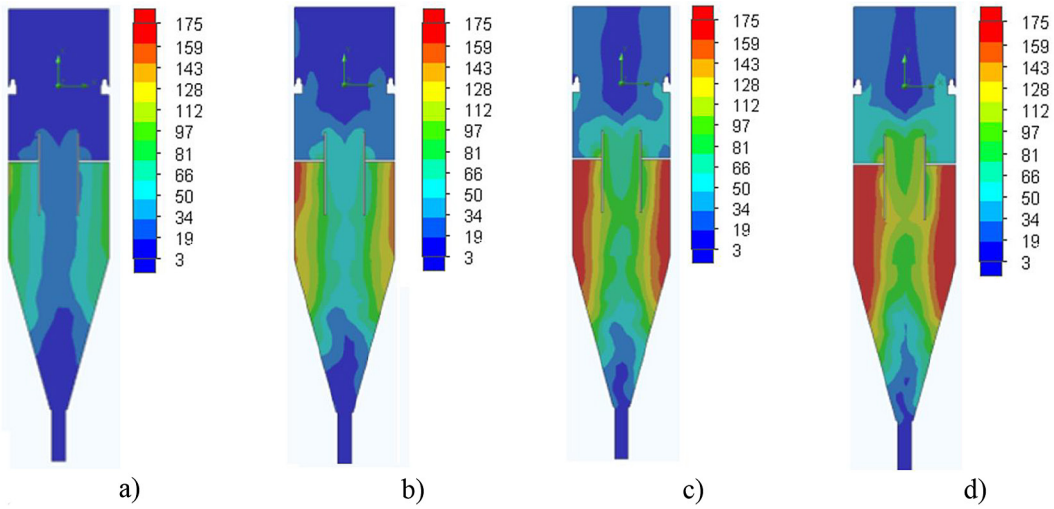

Figure 3. Distribution of gas velocity (m/s) in the cross-section of the cyclone; (a) 0.065 m^3/s; (b) 0.13 m^3/s; (c) 0.195 m^3/s; (d) 0.026 m^3/s

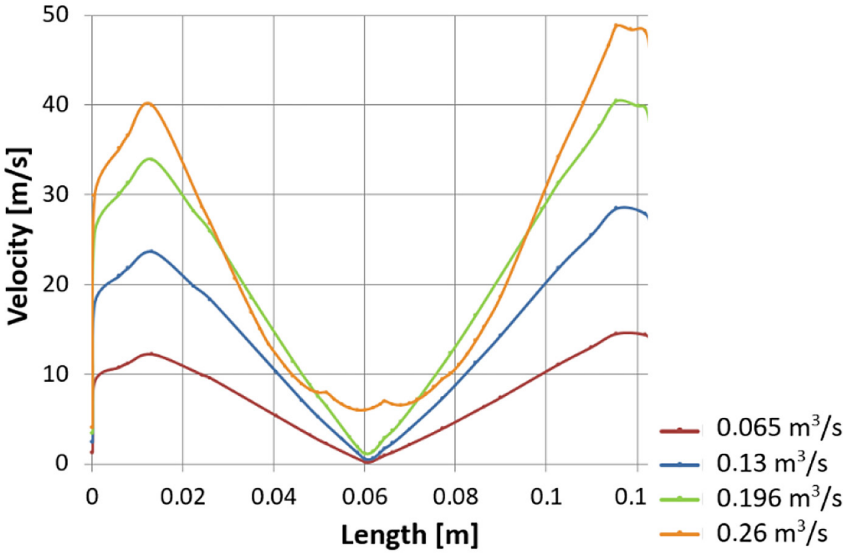

Figure 5. Distribution of gas mixture velocity along the auxiliary line

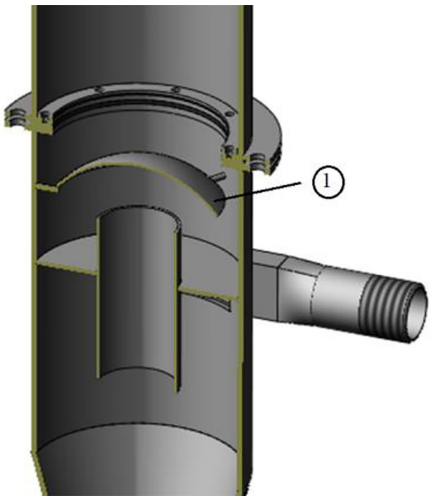

Figure 6. Deflector installed above the outlet nozzle of the cyclone, 1 – deflector

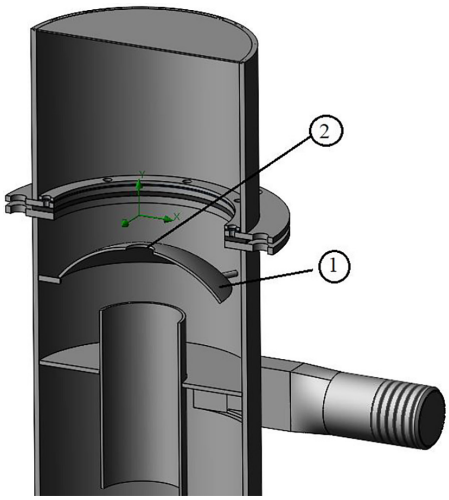

Figure 8. Optimized deflector installed above the outlet nozzle of the cyclone, 1 – deflector; 2 – hole in the deflector

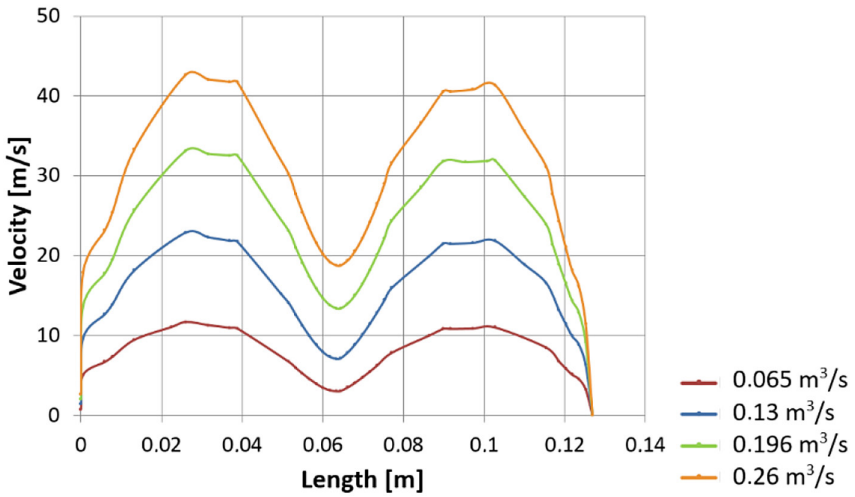

Figure 7. Distribution of gas mixture velocity along the auxiliary line

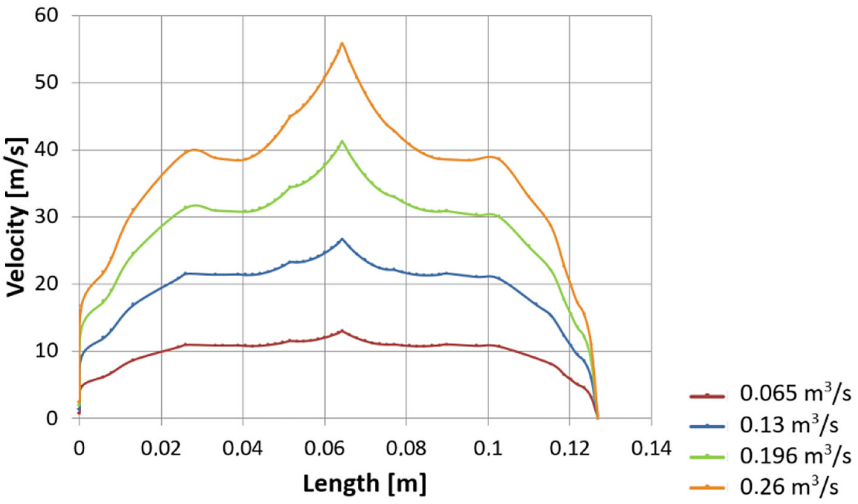

Figure 9. Distribution of gas mixture velocity along the auxiliary line

above the outlet nozzle of the cyclone is proposed (Figure 6). Figure 7 illustrates the distribution of gas velocity along the auxiliary line with the implementation of this deflector.

According to the results illustrated in Figure 7, the velocity distribution in the cross-section of the cyclone, where a deflector is installed above the outlet nozzle, remains non-uniform, although it shows significant improvement compared with the cyclone without a deflector. It is important to note that the gas mixture flow rate influences the velocity distribution in the longitudinal section of the cyclone. Specifically, an increase in flow rate exacerbates the non-uniformity in the velocity distribution across the transverse section of the cyclone. Given the operating flow rate of the adsorber, which is 0.13 m³/s, the current deflector design in the adsorber is ineffective. To enhance its efficiency, it is proposed to incorporate a through hole in the deflector (Figure 8). Simulations of the cyclone with the improved deflector design are presented in Figure 9.

Hence, the hole in the deflector, installed above the outlet nozzle of the cyclone, significantly changed the velocity distribution along the auxiliary line. By fine-tuning the location, geometry, and size of the aperture, the velocity distribution along the auxiliary line can be made even more uniform, which will be implemented in further studies.

CONCLUSIONS

The current adsorber designs exhibit complexity, large size, and low efficiency. In response to that, a modular laboratory adsorber design has been developed, comprising five sections that can be adjusted in quantity as required. Future iterations of the adsorber may incorporate monitoring and measurement instruments to facilitate laboratory research on carbon dioxide capture from gas mixtures using zeolite as the adsorbent.

To optimize the adsorber efficiency, particularly in achieving uniform gas flow across the transverse section of the cyclone outlet, simulation studies were conducted. These studies examined various factors, such as gas flow rates, shapes, designs, and sizes, both with and without additional distribution elements. Among the proposed solutions, it was found that the installation of a hemispherical deflector above the cyclone outlet, featuring a central hole, achieves the most uniform gas distribution. This design offers simplicity, robust performance across varying gas flow rates, and advanced manufacturing feasibility compared with alternative options.

Further research on the developed adsorber will focus on studying its operation. A full-scale model of the adsorber will be fabricated, and a series of experimental studies will be conducted to determine its technical and technological characteristics, as well as to evaluate the properties of the adsorbents under various gas mixture parameters.

Acknowledgments

The present article originated as part of the research internships "Using advanced FEM modeling to simulate mechanical engineering processes" by Vasyl Mykhailiuk and "Solving

optimization problems in mechanical engineering using advanced FEM modeling" by Ruslan Deineha at the AGH University of Krakow, Faculty of Mechanical Engineering and Robotics, Department of Manufacturing Systems.

REFERENCES

1. Grandhi S., Viswanadham M. Simulation of carbon dioxide capture by adsorption on activated carbon. Journal of Applied Geochemistry 2015; 17: 432–436.
2. Yu C.H., Huang C.H., Tan C.S. A review of CO_2 capture by absorption and adsorption. Aerosol and Air Quality Research 2012; 12. https://doi.org/10.4209/aaqr.2012.05.0132
3. Shamiri A., Shafeeyan M.S. Evaluation of adsorbent materials for carbon dioxide capture. Materialwissenschaft und Werkstofftechnik 2022; 53(11): 1392–1409. https://doi.org/10.1002/mawe.202100332
4. Chávez R.H., Guadarrama J.d.J., Klapp J. CO_2 capture for atmosphere pollution reduction. In: Klapp J, Cervantes-Cota JL, Chávez Alcalá JF, editors. Towards a Cleaner Planet: Energy for the Future [Internet] Berlin, Heidelberg: Springer; 2007 [cited 2024 May 21]. 99–111. Available from: https://doi.org/10.1007/978-3-540-71345-6_8
5. Lee, S.Y., Park, S.J. A review on solid adsorbents for carbon dioxide capture. Journal of Industrial and Engineering Chemistry 2015; 23: 1–11.
6. Reddy M.S.B., Ponnamma D., Sadasivuni K.K., Kumar B., Abdullah A.M. Carbon dioxide adsorption based on porous materials. RSC Advances 2021; 11: 12658–12681. https://doi.org/10.1039/D0RA10902A
7. Wahono S., Stalin J., Addai-Mensah J., Skinner W., Vinu A., Vasilev K. Physico-chemical modification of natural mordenite-clinoptilolite zeolites and their enhanced CO_2 adsorption capacity. Microporous and Mesoporous Materials 2019; 294: 109871. https://doi.org/10.1016/j.micromeso.2019.109871
8. Pérez-Botella E., Valencia S., Rey F. Zeolites in adsorption processes: State of the art and future prospects. Chemical Reviews 2022; 122(24): 17647–17695. https://doi.org/10.1021/acs.chemrev.2c00140
9. Podzharskyi M.A. Theoretical Foundations of Sorption Processes: Lecture Notes. Dnipro: Publishing House of Dnipropetrovsk National University; 2007 (in Ukrainian).
10. Huang H., He Z., Yuan H., Kobayashi N., Zhao D., Kubot, M., Guo H. Effect of adsorbent diameter on the performance of adsorption refrigeration. Chinese Journal of Chemical Engineering 2014; 22(5): 602–606. https://doi.org/10.1016/S1004-9541(14)60074-4
11. Verde M., Harby K., Corberán J.M. Optimization of thermal design and geometrical parameters of a flat tube-fin adsorbent bed for automobile air-conditioning. Applied Thermal Engineering 2017; 111: 489–502. https://doi.org/10.1016/j.applthermaleng.2016.09.099
12. Sosnowski M., Grabowska K., Krzywanski J., Nowak W., Sztekler K. Kalawa, W. The effect of heat exchanger geometry on adsorption chiller performance. Journal of Physics: Conference Series 2018; 1101: 012037. https://doi.org/10.1088/1742-6596/1101/1/012037
13. Kler S.C., Lavin J.T. Computer simulation of gas distribution in large shallow packed adsorbers. Gas Separation & Purification 1987; 1(1): 55–61. https://doi.org/10.1016/0950-4214(87)80009-9
14. Fleischer F., Koerner C., Mann J. Flow guiding and distributing devices on the exhaust side of stationary gas turbines. Journal of Engineering for Gas Turbines and Power 1990; 112(1): 80–85. https://doi.org/10.1115/1.2906481
15. Li Y., Si H., Wang B., Xue L., Wu X. Optimization design research of air flow distribution in vertical radial flow adsorbers. Korean Journal of Chemical Engineering 2018; 35: 835–846. https://doi.org/10.1007/s11814-017-0348-y
16. Sklepova S.V., Ivanichok N., Kolkovskyi P., Kotsyubynsky V., Boychuk V., Rachiy B., Uhryński A., Bembenek M., Ropyak L. Porous structure and fractal dimensions of activated carbon prepared from waste coffee grounds. Materials 2023; 16(18): 6127. https://doi.org/10.3390/ma16186127
17. Bembenek M., Kotsyubynsky V., Boychuk V., Rachiy B., Budzulyak I., Kowalski Ł., Ropyak L. Effect of synthesis conditions on capacitive properties of porous carbon derived from hemp bast fiber. Energies 2022; 15(22): 8761. https://doi.org/10.3390/en15228761
18. Cherniuk V.V., Ivaniv V.V., Bihun I.V., Wojtowicz J.M. Coefficient of flow rate of inlet cylindrical nozzles with lateral orthogonal inflow. In: Proceedings of CEE 2019: Lecture Notes in Civil Engineering.
19. Li Q., He X., Chen Y., Lin J., Zhang Y., Chen R., Zhou X. Numerical study on effects of geometric parameters on the release characteristics of straight sudden expansion gas extinguishing nozzles. Symmetry 2021; 13: 2440. https://doi.org/10.3390/sym13122440
20. Onyshchuk O.O., Kormosh Z.O. Processes and Apparatuses of Chemical Production: Course of Lectures.
21. Technology of Adsorption Gas Drying—Essays and Study Materials on um.co.ua. 2022. http://um.co.ua/2/2-6/2-66347.html (Accessed: 29.05.2024) (in Ukrainian).

22. Ruthven D.M. Principles of adsorption and adsorption processes. John Wiley & Sons; 1984.
23. Liu Y., Zheng X., Dai R. Numerical study of flow maldistribution and depressurization strategies in a small-scale axial adsorber. Adsorption 2014; 20: 757–768. https://doi.org/10.1007/s10450-014-9619-7
24. Yang R.T. Gas separation by adsorption processes. 1, World Scientific; 1997.
25. Brunke J.C., Blesl M. Energy conservation measures for the German cement industry and their ability to compensate for rising energy-related production costs. Journal of Cleaner Production 2014; 82: 94–111. https://doi.org/10.1016/j.jclepro.2014.06.074
26. Liu X., Yuan Z., Xu Y., Jiang S. Greening cement in China: A cost-effective roadmap. Applied Energy 2017; 189: 233–244. https://doi.org/10.1016/j.apenergy.2016.12.057
27. Hamad M.A., Nasr M., Shubbar A., Al-Khafaji Z., Al Masoodi Z., Al-Hashimi O., Kot P., Alkhaddar R., Hashim K. Production of ultra-high-performance concrete with low energy consumption and carbon footprint using supplementary cementitious materials instead of silica fume: A review. Energies 2021; 14(24): 8291. https://doi.org/10.3390/en14248291
28. Aitcin P. Cements of yesterday and today: Concrete of tomorrow. Cement and Concrete Research 2000; 30: 1349–1359. https://doi.org/10.1016/S0008-8846(00)00365-3
29. Oss H.V., Padovani A.C. Cement manufacture and the environment: Part I: Chemistry and Technology. Journal of Industrial Ecology 2002; 6. https://doi.org/10.1162/108819802320971650
30. Cleary P. Axial transport in dry ball mills. Applied Mathematical Modelling 2006; 30: 1343–1355. https://doi.org/10.1016/j.apm.2006.03.018
31. Cui H., Yuan Z.G., Feng Z. Data-driven Modeling of Ball Mill Load and Cement Particle Size. In: 2018 Chinese Automation Congress (CAC) [Internet] 2018 [cited 2024 May 24]. 3913–3917. Available from: https://ieeexplore.ieee.org/document/8623461
32. Ghalandari V., Iranmanesh A. Energy and exergy analyses for a cement ball mill of a new generation cement plant and optimizing grinding process: A case study. Advanced Powder Technology 2020; 31(5): 1796–1810. https://doi.org/10.1016/j.apt.2020.02.013
33. Plashykhin S.V. Handbook on Resource-Efficient and Clean Production. Cement Industry. Kyiv: Center for Resource-Efficient and Clean Production; 2020, 96 (in Ukrainian).
34. Schuhmacher M., Domingo J.L., Garreta J. Pollutants emitted by a cement plant: health risks for the population living in the neighborhood. Environmental Research 2004; 95(2): 198–206. https://doi.org/10.1016/j.envres.2003.08.011
35. Lei Y., Zhang Q., Nielsen C., He K. An inventory of primary air pollutants and CO_2 emissions from cement production in China, 1990–2020. Atmospheric Environment 2011; 45(1): 147–154. https://doi.org/10.1016/j.atmosenv.2010.09.034
36. Guo Z., Bai X., Liu S., Luo L., Hao Y., Yunqian L., Xiao Y., Yang J., Tian H.Z. Heterogeneous variations on historical and future trends of CO_2 and multiple air pollutants from the cement production process in China: emission inventory, spatial–temporal characteristics, and scenario projections. Environmental Science & Technology 2022; 56. https://doi.org/10.1021/acs.est.2c04445
37. Monkman S., Shao Y. Carbonation curing of slag-cement concrete for binding CO_2 and improving performance. Journal of Materials in Civil Engineering 2010; 22(4): 296–304. https://doi.org/10.1061/(ASCE)MT.1943-5533.0000018
38. Scrivener K.L., John V.M., Gartner E.M. Eco-efficient cements: Potential economically viable solutions for a low-CO_2 cement-based materials industry. Cement and Concrete Research 2018; 114: 2–26. https://doi.org/10.1016/j.cemconres.2018.03.015
39. Herzog H.J., Golomb D.S. Carbon capture and storage from fossil fuel use. In: Encyclopedia of Energy Elsevier; 2004; 277–287.
40. IPCC Special Report on Carbon Dioxide Capture and Storage. Metz B., Davidson O., de Coninck H.C., Loos M., Meyer L.A., editors. Cambridge: Cambridge University Press; 2005.
41. Moritis G. CO_2 injection gains momentum. Oil & Gas Journal 2006; 104(15): 37–41.
42. Alvarado V., Manrique E. Enhanced oil recovery: Field planning and development strategies. Gulf Professional Publishing; 2010.
43. Enick R.M., Klara S.M. CO_2 solubility in water and brine under reservoir conditions. Chemical Engineering Communications 1990; 90(1): 23–33. https://doi.org/10.1080/00986449008940574
44. Thomas S. Enhanced oil recovery—An overview. Oil & Gas Science and Technology 2008; 63(1): 9–19. https://doi.org/10.2516/ogst:2007060
45. McGlade C., Speirs J., Sorrell S. Unconventional gas—A review of regional and global resource estimates. Energy 2013; 55: 571–584. https://doi.org/10.1016/j.energy.2013.01.048
46. Global CCS Institute. The global status of CCS 2020 [Internet]. 2020. Available from: https://www.globalccsinstitute.com/wp-content/uploads/2021/03/Global-Status-of-CCS-Report-English.pdf
47. Mykhailiuk V.V., Liakh M.M., Protsiuk V.R., Faflei O.Y., Protsiuk G.Y., Deineha P.O. Separator for Separating Water Vapor Condensate from Flue

Gases in Cement Production. In: The Current State of Development of World Science: Characteristics and Features Lisbon, Portuguese Republic: International Center of Scientific Research 2023; 108–113.

48. Kolle J.M., Fayaz M., Sayari A. Understanding the Effect of Water on CO_2 Adsorption. Chemical Reviews 2021; 121(13): 7280–7345. https://doi.org/10.1021/acs.chemrev.0c00762
49. Katare P., Krupan A., Dewasthale A., Datar A., Dalkilic A.S. CFD analysis of cyclone separator used for fine filtration in separation industry. Case Studies in Thermal Engineering 2021; 28: 101384. https://doi.org/10.1016/j.csite.2021.101384
50. Chu K.W., Wang B., Xu D.L., Chen Y.X., Yu A.B. CFD–DEM simulation of the gas–solid flow in a cyclone separator. Chemical Engineering Science 2011; 66(5): 834–847.
51. Kryzhanivskyi Y.I., Liakh M.M., Mykhailiuk V.V., Makoviychuk M.V., Kuchirka Y.M., Vytrekhovskyi Y.A. Method for separating liquid and mechanical particles from a gas stream. 152837, 2023 (in Ukrainian).
52. Katopodes N.D. Free-surface flow: computational methods. Butterworth-Heinemann; 2018.
53. Dragan V., Malael I., Gherman G.B. A comparative analysis between optimized and baseline high pressure compressor stages using tridimensional computational fluid dynamics. Engineering, Technology & Applied Science Research 2016; 6(4): 1103–1108. https://doi.org/10.48084/etasr.696
54. Maistruk V.V., Havryliv R.I., Popil A.S., Basistyi A.M. Evaluation of energy costs in the operation of a direct-flow cyclone using the FLOW SIMULATION software package. Eastern-European Journal of Advanced Technologies 2012; 6/8(60): 28–30 (in Ukrainian).
55. Lucas F., Huebner R. Numerical simulation of single-phase and two-phase flows in separator vessels with inclined half-pipe inlet device applied in reciprocating compressors. Engineering, Technology & Applied Science Research 2018; 8: 2897–2900. https://doi.org/10.48084/etasr.1993
56. Flow Simulation. Technical reference solidworks flow simulation 2021, 2020. https://www.cati.com/wp-content/uploads/2021/04/swflow2021-technical-reference.pdf (Accessed: 29.05.2024)